J Mater Sci (2007) 42:10203–10218
DOI 10.1007/s10853-007-1979-x

Crystallization of $CaHf_{1-x}Zr_xTi_2O_7$ ($0 \leq x \leq 1$) zirconolite in SiO_2–Al_2O_3–CaO–Na_2O–TiO_2–HfO_2–ZrO_2–Nd_2O_3 glasses

Daniel Caurant · Isabelle Bardez · Pascal Loiseau

Received: 20 March 2007 / Accepted: 2 July 2007 / Published online: 5 September 2007

Abstract Glass-ceramics containing (Hf,Zr)-zirconolite crystals (nominally $CaHf_{1-x}Zr_xTi_2O_7$ with $0 \leq x \leq 1$) were envisaged to immobilize minor actinides and plutonium. Such materials were prepared in this study by controlled crystallization of glasses belonging to the SiO_2–Al_2O_3–CaO–Na_2O–TiO_2–HfO_2–ZrO_2–Nd_2O_3 system. Neodymium was used as trivalent actinides surrogate. The effect of total or partial substitution of ZrO_2 by HfO_2 (neutron poison for fission reactions) on glass crystallization in the bulk and near the surface is presented. It appeared that Hf/Zr substitution had not significant effect on nature, structure, and composition of crystals formed both on glass surface (titanite + anorthite) and in the bulk (zirconolite). This result can be explained by the close properties of Zr^{4+} and Hf^{4+} ions and by their similar structural role in glass structure. However, strong differences were observed between the nucleation rate I_Z of zirconolite crystals in glasses containing only HfO_2 and in glasses containing only ZrO_2. Hf-zirconolite ($CaHfTi_2O_7$) crystals were shown to nucleate only very slowly in comparison with Zr-zirconolite ($CaZrTi_2O_7$) crystals. Composition changes - by increasing either HfO_2 or Al_2O_3 concentration or by introducing ZrO_2 in parent glass - were performed to increase I_Z in hafnium-rich glasses. The proportion of Nd^{3+} ions incorporated in the zirconolite phase was estimated using ESR.

D. Caurant (✉) · I. Bardez · P. Loiseau
Laboratoire de Chimie de la Matière Condensée de Paris, UMR-CNRS 7574, Ecole Nationale Supérieure de Chimie de Paris (ENSCP, ParisTech), 11 rue Pierre et Marie Curie, 75231 Paris, France
e-mail: daniel-caurant@enscp.fr

Present Address:
I. Bardez
Commissariat à l'Energie Atomique Valrho, 30207 Marcoule, Bagnols-sur-Ceze, France

Introduction

Artificial actinides such as Pu, Np, Am, and Cm are generated by neutron capture in nuclear power reactors during electricity production and in military reactors during Pu production. After the reprocessing of power plants and military spent fuels, high level radioactive waste solutions (HLW) containing fission products FP and minor actinides MA (Np, Am, Cm) are recovered that must be immobilized by dissolution in highly durable solid matrices [1–5]. The same problem also exists for Pu-rich wastes such as excess weapons plutonium in several countries (USA, Russia) [6, 7]. The selected waste forms must exhibit excellent long-term performances in order to isolate the long-lived radionuclides from the biosphere for periods sufficiently long (at least for several 10,000 years) to permit their safe decay during underground disposal. Currently, low melting temperature ($T < 1{,}100$–$1{,}150$ °C) borosilicate and phosphate glasses represent the only waste forms produced industrially to immobilize civil and military HLW (non-separated FP + MA) [1, 3]. However, due to the main contribution of MA to long-term radiotoxicity of HLW, researches are in progress in several countries in order to separate the MA from FP and to immobilize them in specific matrices [8–14]. In this case, due to the absence of volatile element (such as Cs, Ru...) in separated wastes, more refractory host matrices (refractory glasses, ceramics or glass-ceramics) can be envisaged. Among the different matrices reported in literature for the specific incorporation of MA,

phosphate, titanate and zirconate crystalline phases appear among the most chemically durable ones [10, 13, 15]. For instance, Zr-zirconolite (nominally $CaZrTi_2O_7$) ceramic appears as a very good candidate for actinides immobilization due to both the high incorporation capacity and the very good long-term behavior of this phase in spite of its tendency to amorphization under actinides alpha decay [16–20]. Zr-zirconolite is also one of the main phases well known in the multi-phase Australian SYNROC ceramics proposed for the immobilization of non-separated HLW [15, 21]. However, ceramics are not currently used industrially as host matrices for the immobilization of highly radioactive radionuclides partly because of the existence of technological difficulties to prepare single-phase ceramics either by melting (zirconolite does not melt congruently [22]) or by sintering (risk of formation of less durable parasitic phases able to incorporate radionuclides). In comparison, glass-ceramics prepared either by controlled crystallization of a glass or by slow cooling of a melt could be obtained more easily than single-phase ceramic waste forms in nuclear facilities [23, 24]. Moreover, because of the existence of a residual glassy phase, glass-ceramic waste forms could accommodate more easily than ceramics the composition waste variations and the presence of impurities.

In other studies, the possibility to prepare highly durable glass-ceramics containing Zr-zirconolite crystals in their bulk was demonstrated by controlled crystallization (nucleation + crystal growth) of parent glass compositions belonging to the SiO_2–Al_2O_3–CaO–Na_2O–TiO_2–ZrO_2–Ln_2O_3 (Ln: lanthanides) system [4, 25–30]. In these works, trivalent lanthanide ions such as Nd^{3+} were used as MA surrogate due to their similar charge and radii in comparison with MA. In this case, it was shown that a significant fraction of lanthanide ions was incorporated in Zr-zirconolite crystals (double containment principle) [4, 25, 29, 30]. Moreover, it was shown that the amount of Ln^{3+} cations incorporated in the Ca and Zr sites of the Zr-zirconolite crystals of the glass-ceramics strongly depended on Ln^{3+} field strength [29, 30]. The ability of the zirconolite phase of the glass-ceramics to incorporate natural (Th) and artificial actinides (Pu) was also demonstrated [4, 20, 30, 31].

As Zr^{4+} and Hf^{4+} ions have nearly identical radii (respectively 0.78 and 0.76 Å in 7-fold coordination [32] as in zirconolite structure) and belong to the same column of the periodic table, these two elements have very similar chemical properties and are expected to be incorporated in similar crystalline structures and to play similar roles in the glassy network. Indeed, previous works revealed that it was possible to prepare (Zr,Hf)-zirconolite $CaZr_{1-x}Hf_xTi_2O_7$ ($0 \leq x \leq 1$) [33–36] and Nd-doped Hf-zirconolite $Ca_{1-x}Nd_xHfTi_{2-x}Al_xO_7$ ($0 < x \leq 0.2$) [37, 38] ceramic samples. These studies also showed that the crystalline structure of Hf- and Zr-zirconolite were very similar and that the environment of Nd^{3+} ions was the same in these two ceramics [37, 38]. Moreover, the chemical durabilities of Zr- and Hf-zirconolite ceramics (dissolution rates of Hf and Zr) are very similar [39, 40]. As hafnium has a higher thermal neutron capture cross-section than zirconium (respectively 104 and 0.184 barns [41]), it is considered as a neutron poison for fission reactions. Moreover, several authors also considered hafnium as a surrogate for Pu^{4+} [42]. Even if hafnium remains significantly more expensive than zirconium, it could be interesting to substitute either totally or partially Zr by Hf in zirconolite crystals of the glass-ceramics to prevent criticality events in waste forms heavily loaded with fissile actinide isotopes such as ^{239}Pu.

The results of thermochemical investigations on Hf-zirconolite ceramic indicated that this crystalline phase was thermodynamically more stable than Zr-zirconolite which could be another advantage of the Hf/Zr substitution [36]. However, a more recent paper published by the same laboratory [43] indicated that the results reported in [36] were in error due to the underestimation of the enthalpy of formation of $CaHfTi_2O_7$. This could modify the relative stability of $CaHfTi_2O_7$ and $CaZrTi_2O_7$ reported in [36]. Other studies about actinide host phases showed that it was possible to synthesize $La_2Zr_2O_7$ and $La_2Hf_2O_7$ ceramics with pyrochlore structure [44]. Lumpkin et al. [44] indicated that the substitution of Zr by Hf in $La_2Zr_2O_7$ structure had a significant impact on the critical amorphization dose under heavy ion irradiation. However, to the best of our knowledge such a comparison of Zr- and Hf-zirconolite behavior under ion irradiation was not performed.

The main goal of this paper was to study the possibility to prepare (Hf,Zr)-zirconolite ($CaHf_{1-x}Zr_xTi_2Al_xO_7$ with $0 \leq x < 1$) based glass-ceramics replacing either partially or totally Zr by Hf in the parent glass composition studied in previous works [26, 45]. Neodymium was used as trivalent actinides surrogate in SiO_2–Al_2O_3–CaO–Na_2O–TiO_2–HfO_2–ZrO_2–Nd_2O_3 parent glasses. Using a two-step glass-ceramic process, the nucleation and crystal growth of (Hf,Zr)-zirconolite crystals (with $x \neq 1$) in the bulk are compared to that of Zr-zirconolite crystals (with $x = 1$) in glass compositions containing only ZrO_2. Several composition changes have also been performed in order to increase the nucleation rate I_Z of (Hf,Zr)-zirconolite ($x \neq 1$). To estimate the amount of Nd^{3+} ions incorporated in zirconolite crystals, Electron Spin Resonance (ESR) and Electron Probe Microanalysis (EPMA) were used. Moreover, the presence of silicate crystalline phases (titanite + anorthite) growing from glass surface was also studied and the results were compared with that obtained for the glass containing only ZrO_2.

Experimental procedure

Preparation of glasses

In order to study the effect of partial or total substitution of Zr by Hf (in mol.%) in parent glass on its crystallization behavior (nature of phases crystallizing in the bulk and from the surface, nucleation, and crystal growth rates) six glasses containing either a mixture $HfO_2 + ZrO_2$ or only HfO_2 were prepared (Table 1). The compositions of two glasses GZr and GZr(Nd) containing only ZrO_2 with respectively 0 and 6 wt% Nd_2O_3 prepared for previous studies are also reported in Table 1. Glass compositions GHf and $GHf(Nd)_a$ (with only hafnium) corresponded respectively to compositions GZr and GZr(Nd) (with only zirconium). Glass compositions $GHf(Nd)_b$ and $GHf(Nd)_c$ were derived from composition $GHf(Nd)_a$ increasing respectively HfO_2 and Al_2O_3 concentrations. Glass composition $GHfZr(Nd)_a$ was deduced from composition $GHf(Nd)_a$ replacing half of HfO_2 by ZrO_2 on molar basis. Glass composition $GHfZr(Nd)_b$ was derived from composition $GHf(Nd)_b$ replacing two thirds of HfO_2 by ZrO_2 on molar basis. For all the Nd-doped glasses, the amount of Nd_2O_3 was kept almost constant (1.24–1.27 wt%) and was equivalent to approximately 9.2 wt% Am_2O_3 on molar basis. This amount corresponds to the aimed incorporation level of minor actinides in such specific waste forms.

These different glass compositions can be considered as $(TiO_2,(Hf,Zr)O_2)$-rich SiO_2–Al_2O_3–CaO–Na_2O–Nd_2O_3 glasses with very low Na_2O concentration ($[Na_2O] \leq 1$ wt%). Na_2O was introduced as tracer element in all glass compositions in order to perform chemical durability tests on both parent glasses and glass-ceramics that are not presented in this paper. The projection of glass compositions on the SiO_2–Al_2O_3–CaO ternary phase diagram is located near the silica-rich eutectic point [46]. Glasses belonging to this ternary system are known to be relatively easy to melt (this is the case for instance of the well-known E-glass composition used industrially as reinforcement fibers [47]) and to exhibit good chemical durability and low bulk crystallization tendency. However, HfO_2, ZrO_2, and Nd_2O_3 introduction in this system is expected to increase its liquidus temperature because of the high melting point of these oxides. Moreover, TiO_2 and ZrO_2 are known for their role as nucleating agents in industrial glass-ceramics [48, 49].

The glass preparation method used in this study is the following [26]:

- For each composition, a 50 g batch containing dehydrated reagent-grade SiO_2, Al_2O_3, $CaCO_3$, TiO_2, ZrO_2, HfO_2, Na_2CO_3, and Nd_2O_3 raw materials was melted and refined at 1,550 °C for 10 h in platinum crucible using an electric furnace.
- Pouring of the melt in water and grinding in order to obtain more homogeneous glasses after a second melting.
- Second melting at 1,550 °C for 4 h and casting in steel cylinders of 1 cm diameter and height.
- Annealing at 775 °C (near the glass transformation temperature range $T_g \sim 760$ °C) and slow cooling to room temperature in order to relieve internal stresses before cutting.

Table 1 Composition (wt. and mol.%) of parent glasses (target compositions)

Glass reference	Composition	SiO_2	Al_2O_3	CaO	TiO_2	ZrO_2	HfO_2	Nd_2O_3	Na_2O	T_g (°C)
GHf	wt.%	40.57	11.95	19.63	12.46	0.00	14.45	0.000	0.94	762 ± 2
	mol.%	48.85	8.48	25.33	11.28	0.00	4.97	0.000	1.09	
$GHf(Nd)_a$	wt.%	38.27	11.27	18.52	11.75	0.00	13.64	5.66	0.89	765 ± 2
	mol.%	48.23	8.37	25.00	11.14	0.00	4.91	1.27	1.08	
$GHf(Nd)_b$	wt.%	35.83	10.55	17.34	11.00	0.00	19.15	5.30	0.83	–
	mol.%	47.07	8.17	24.41	10.87	0.00	7.18	1.24	1.06	
$GHf(Nd)_c$	wt.%	36.71	14.64	17.77	11.27	0.00	13.08	5.67	0.85	–
	mol.%	46.81	11.00	24.27	10.81	0.00	4.76	1.29	1.05	
$GZrHf(Nd)_a$	wt.%	39.38	11.60	19.06	12.09	4.11	7.02	5.83	0.91	763 ± 2
	mol.%	48.22	8.37	25.00	11.14	2.45	2.45	1.27	1.08	
$GZrHf(Nd)_b$	wt.%	37.83	11.14	18.31	11.61	7.89	6.74	5.59	0.88	–
	mol.%	47.07	8.17	24.41	10.87	4.79	2.39	1.24	1.06	
GZr	wt.%	43.15	12.71	20.88	13.25	9.00	0.00	0.00	1.00	761 ± 2
	mol.%	48.85	8.48	25.33	11.28	4.97	0.00	0.00	1.09	
GZr(Nd)	wt.%	40.57	11.94	19.63	12.45	8.46	0.00	6.000	0.94	761 ± 2
	mol.%	48.23	8.37	25.00	11.14	4.90	0.00	1.27	1.08	

The glass transformation temperature T_g (determined by DTA) is also reported for several samples

It is interesting to notice that contrary to classical borosilicate nuclear glasses currently used for HLW immobilization and melted at temperatures never exceeding 1,100–1,200 °C for technical reasons, the absence of volatile products both in separated wastes (MA, Pu), in simulated ones (lanthanides) and in parent glass batch (expect the low amount of sodium) allows higher melting temperatures in our case (Table 1).

Preparation of glass-ceramics

The glass-ceramics were firstly prepared using the method described in [26] for Zr-zirconolite based glass-ceramics which consisted in a two-step thermal treatment of parent glasses including a 2 h nucleation stage at T_n = 810 °C and a 2 h crystal growth stage at either T_c = 1,050 or 1,200 °C before annealing at 775 °C. Nevertheless, for several samples, the duration of the nucleation and crystal growth steps was increased. The two crystal growth temperatures chosen in this study (T_c = 1,050 and 1,200 °C) were shown to lead to the crystallization of Zr-zirconolite as the only crystalline phase in the bulk of glasses containing only ZrO_2 [25, 30, 45]. However, several heat treatments were also performed at T_c < 1,000 °C for comparison with previous results concerning samples with only ZrO_2. The nucleation rate curve $I_z = f(T)$ of Hf-zirconolite in the bulk of GHf glass was determined and compared with that of GZr(Nd) glass already given in another paper [26]. The $I_z = f(T)$ curve was determined using glass samples nucleated for 24 h at a nucleation temperature (T_n) ranging from 740 to 820 °C. The samples were then heat treated at the crystal growth temperature T_c = 1,050 °C for 1 h to reveal the nuclei formed during the heat treatment at T_n. The value of T_c was chosen in order to minimize the risk of nuclei dissolution during the crystal growth stage in accordance with the results obtained for GZr(Nd) glass [26]. The nucleation rate was then estimated by counting the number of crystals on the scanning electron microscopy (SEM) images (average performed on 12 images) [37]. Because of the slow nucleation rate of zirconolite crystals in the bulk of hafnium-rich glasses (see below), it appeared that it was necessary to increase the nucleation duration (40–50 h) and to perform nucleation at temperature T_n close to that corresponding to the maximum of the $I_z = f(T)$ curve in order to increase the amount of crystalline phase in the bulk of glass-ceramics.

Characterization of glasses and glass-ceramics

In order to determine the glass transformation temperature T_g and to study the glass crystallization behavior, differential thermal analysis (DTA) measurements were performed under air on parent glasses with the help of a NETZSCH STA 409 thermal analysis apparatus (heating rate: 10 °C/min, glass particle size: 125–250 μm). T_g was determined using the onset of the corresponding DTA endothermic effect.

All the partially crystallized samples were characterized by X-ray diffraction (XRD) using a Siemens D5000 apparatus operating at CoK_α wavelength (λ = 1.778897 Å). In order to determine the lattice parameters of Hf-zirconolite crystals for GHf and $GHf(Nd)_a$ samples, the glasses were nucleated at T_n = 770 °C during 48 h and the crystals were grown at T_c = 1,050 °C during 4 h. These heat treatment conditions enabled to obtain a higher quantity of zirconolite and to record a stronger XRD pattern from which were then extracted the lattice parameters by refinement using a least-squares procedure. The bulk and the surface of glass-ceramics were studied by scanning electron microscopy (SEM) and energy dispersive X-ray analysis (EDX) on polished and carbon coated samples using a Hitachi S2500 microscope equipped with a PGT analyzer (accelerating voltage 15 kV, beam current ≈ 1.8 nA). However, because of the lack of resolution by EDX between the strongest hafnium M lines (M_1(Hf) = 1,645 eV, M_2(Hf) = 1,698 eV), the silicon $K_{\alpha 1}$ line ($K_{\alpha 1}$(Si) = 1,740 eV) and the aluminum $K_{\alpha 1}$ line ($K_{\alpha 1}$(Al) = 1,487 eV), it was not possible to determine correctly the composition of parent glasses and crystals containing both Hf and (Al,Si). Nevertheless, EDX spectra were recorded to study qualitatively the samples. The same problem already occurred during the EDX study of Nd-doped Hf-zirconolite $Ca_{1-y}Nd_yHfTi_{2-y}Al_yO_7$ ($y \neq 0$) ceramics [38]. In order to get quantitative results, we carried out EPMA analysis with the help of a Cameca SX50 apparatus (accelerating voltage 15 kV, beam current 15 nA). Due to the high resolution of this technique, the composition of glasses and crystals were accurately determined. EDX and EPMA analysis were only performed for the glass-ceramic samples prepared at T_c = 1,200 °C for which crystals were large enough to be probed by the electron beam.

An ESR spectrometer Bruker ESP 300e operating at X-band ($\nu \sim 9.5$ GHz) and equipped with a TE102 rectangular cavity and an Oxford variable temperature accessory was used to follow the incorporation and to estimate the amount of paramagnetic Nd^{3+} ions ($4f^3$) in zirconolite crystals formed in the bulk of glass-ceramics. Due to the very short spin-lattice relaxation time T_1 of neodymium at room temperature, ESR spectra were all recorded at low temperature (T = 12 K). We showed that the ESR signal of Nd^{3+} ions in glass-ceramics can be simulated as a linear combination of two neodymium signals: the first one corresponding to Nd^{3+} ions remaining in residual glass whose spectrum was close to that of parent glass, and the second one corresponding to neodymium incorporated in

the zirconolite crystalline phase [28]. A quantitative analysis of ESR spectra can be then performed in order to estimate the total amount of neodymium incorporated into the zirconolite crystals of the bulk. A partitioning ratio R, equal to the molar fraction of Nd^{3+} ions incorporated into the zirconolite phase versus total Nd^{3+} amount, was then calculated. As the double integral of ESR spectra is proportional to the quantity of probed paramagnetic ions (Nd^{3+}), R was calculated by dividing the double integral S_Z of the signal associated with zirconolite (isolated from residual glass contribution) by the double integral S_{GC} of global spectrum including residual glass and zirconolite contributions: $R = S_Z/S_{GC}$.

Optical absorption spectra of Nd^{3+} ions were recorded with a Varian Cary 5E double beam spectrometer at T = 300 K on polished parent glass samples (thickness = 0.52 mm). At this temperature, the optical transitions to excited states from the lowest and from higher Stark doublets of $^4I_{9/2}$ ground state are both observed. Neodymium fluorescence spectra ($^4F_{3/2} \rightarrow {}^4I_{9/2}$ transition) of parent glasses were recorded at T < 20 K after excitation with a tunable Ti-Sa laser in the $^4I_{9/2} \rightarrow {}^4F_{5/2},{}^2H_{9/2}$ region (~806.5 nm) of the absorption spectrum (Fig. 1). When T < 20 K, fluorescence only occurred from the lowest Stark level of the $^4F_{3/2}$ excited state to the $^4I_{9/2}$ state of neodymium and it is possible to estimate the mean energy differences between the five Stark levels of the $^4I_{9/2}$ state splitted by the low symmetry crystal field around neodymium ions in glasses.

Results and discussions

Study of parent glasses

All glasses were fully transparent and X-ray amorphous. The compositions of several parent glasses analyzed by EPMA are given in Table 2. Target and analyzed glass compositions were very similar. This result is in agreement with the lack of significant amount of volatile element (only sodium in our case) in the melt. T_g did not significantly vary between the different glasses (Table 1), which showed that total or partial substitution of ZrO_2 by HfO_2 has no strong effect on the structure of the glassy network

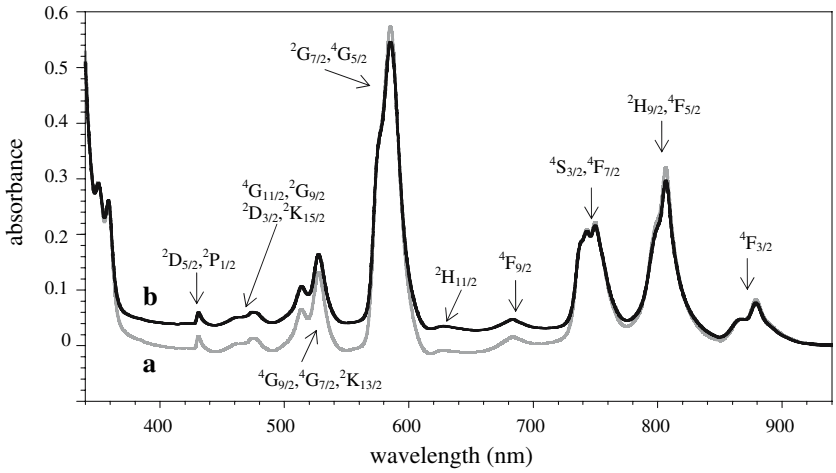

Fig. 1 Optical absorption spectrum of GZr(Nd) (**a**) and $GHf(Nd)_a$ (**b**) parent glasses recorded at 300K. Peak positions and half-width are very similar for the two glasses. Absorption peaks correspond to transitions from the $^4I_{9/2}$ ground state of Nd^{3+} ions to the excited levels indicated in the figure

Table 2 Composition (wt.%) of $GHf(Nd)_a$, $GZrHf(Nd)_a$, $GZrHf(Nd)_b$, and GZr(Nd) parent glasses as analyzed by EPMA

Glass reference	Composition (wt.%)	SiO_2	Al_2O_3	CaO	TiO_2	ZrO_2	HfO_2	Nd_2O_3	Na_2O
$GHf(Nd)_a$	Batch	38.27	11.27	18.52	11.75	0.00	13.64	5.66	0.89
	Analyzed	38.17	10.97	18.84	11.82	0.09	13.49	5.77	0.83
$GZrHf(Nd)_a$	Batch	39.38	11.60	19.06	12.09	4.11	7.02	5.83	0.91
	Analyzed	39.64	12.12	19.17	11.54	4.08	6.63	5.84	0.93
$GZrHf(Nd)_b$	Batch	37.83	11.14	18.31	11.61	7.89	6.74	5.59	0.88
	Analyzed	37.69	10.80	18.42	11.57	8.22	6.64	5.88	0.76
GZr(Nd)	Batch	40.57	11.94	19.63	12.45	8.46	0.00	6.000	0.94
	Analyzed	39.11	11.94	20.02	12.67	9.13	0.01	6.29	0.81

Target compositions (batch) are also given for comparison

(i.e., no effect on the mean bonds strength and network connectivity). This result is not surprising because Zr^{4+} and Hf^{4+} ions have nearly identical radii [32] (Table 3). Consequently, these two cations probably play the same role in glass structure. This conclusion was also suggested by Bihuniak and Condrate [50] from the determination of ZrO_2 and HfO_2 molar volumes in vitreous silica. The similar structural role of Zr^{4+} and Hf^{4+} ions in glasses was confirmed by EXAFS results published in literature on aluminoborosilicate nuclear glasses containing either ZrO_2 [51] or HfO_2 [52, 53]. Indeed, it was shown that Zr^{4+} and Hf^{4+} ions both occurred in 6-fold coordinated sites with distances d(Zr–O) = 2.08 Å and d(Hf–O) = 2.07 Å, respectively (Table 3).

The comparison of ESR (not shown), optical absorption (Fig. 1) and fluorescence (Fig. 2) spectra of GZr(Nd) and $GHf(Nd)_a$ glasses clearly reveals the lack of significant evolution between the two glasses. Thus, the total replacement of ZrO_2 by HfO_2 in glass composition has no significant effect on the environment of Nd^{3+} ions in glass structure. Indeed, ESR, optical absorption, and fluorescence spectroscopies are very sensitive to the local structure around Nd^{3+} ions. Consequently, the total replacement of Zr^{4+} ions by Hf^{4+} ions in the glass compositions studied in this work has no significant effect both on the structure of the glassy network and on the environment of Nd^{3+} ions.

Study of glasses crystallization by DTA

Except for a small shift of exothermic peaks, the DTA curves of GZr(Nd) and $GHf(Nd)_a$ parent glasses were very similar (Fig. 3). For GZr(Nd) glass, A, T, and C exothermic effects were attributed respectively to titanite, anorthite, and defect-fluorite (corresponding to a highly disordered zirconolite structure [27, 54, 55]) crystallization from the surface of glass particles [55]. Comparison of DTA curves indicates that the same kind of surface crystallization occurred for the two glasses. This was confirmed by XRD, SEM, EDX, and EPMA (see below). As exothermic peaks are associated to surface crystallization, the small peak shift observed in Fig. 3 between GZr(Nd) and

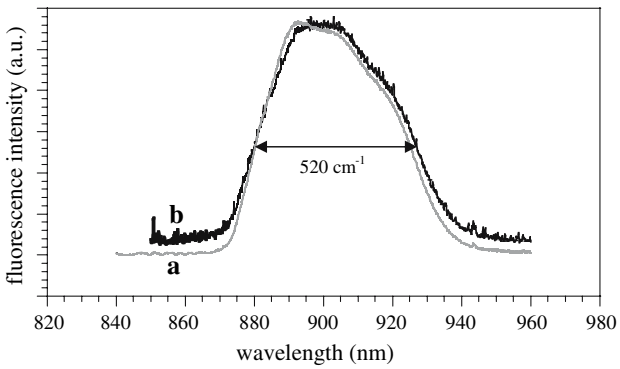

Fig. 2 Fluorescence spectra ($^4F_{3/2} \rightarrow {}^4I_{9/2}$ transition) of GZr(Nd) (**a**) and $GHf(Nd)_a$ (**b**) parent glasses recorded at T < 20 K. The half-width Δ at half-maximum (Δ ~520 cm^{-1}) is almost the same for the two glasses which indicates that replacement of Zr by Hf in glass composition has no significant effect on the crystal field strength around Nd^{3+} ions. Because of the lack of long-range order in glasses, the symmetry around neodymium ions differs slightly from site to site in the glassy network and the observed transitions are inhomogeneously broadened. This explains why, contrary to Nd-doped zirconolite ceramics [37, 38], the five Stark levels of the $^4I_{9/2}$ ground state of neodymium are not resolved in glasses

$GHf(Nd)_a$ parent glasses was probably due to a slight particle size difference between the two powder samples. Indeed, the position of surface crystallization DTA peaks is

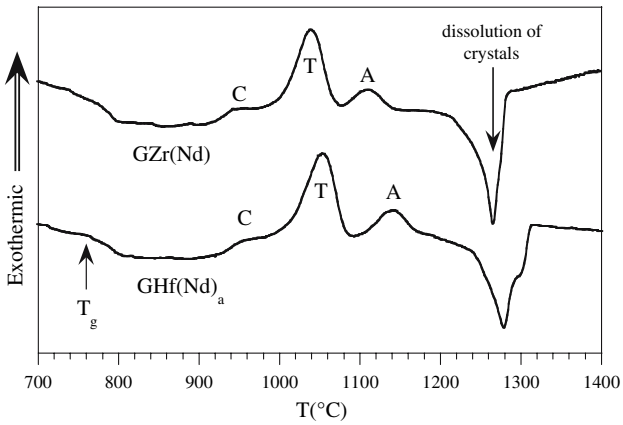

Fig. 3 DTA curves of GZr(Nd) and $GHf(Nd)_a$ parent glasses (size fraction: 125–250 μm, heating rate: 10 °C/min). T: titanite crystallization, A: anorthite crystallization, C: defect-fluorite crystallization

Table 3 Comparison of EXAFS results (Zr K-Edge, Hf-L_3 Edge) obtained for aluminoborosilicate nuclear glasses containing ZrO_2 [51] or HfO_2 [52]

	CN	d(M,O) (Å)	σ^2(Å^2)^a	d(M,Si) (Å)	σ^2(Å^2)^b	R (Å)
Zr^{4+}	6.0	2.08	0.009	3.39	0.004	0.72
Hf^{4+}	6.0	2.07	0.006	3.37	0.006	0.71

CN: coordination number of Zr^{4+} and Hf^{4+} ions with oxygen ions as first neighbor (first shell). d(M,O): Zr–O and Hf–O distances. d(M,Si): Zr–Si and Hf–Si distances with Si as second neighbor (second shell). σ^2: Debye–Waller radial disorder parameters of first (^{a}) and second (^{b}) shells around Zr and Hf. R: Zr^{4+} and Hf^{4+} ions radius in six-fold coordination given by Shannon [32]

known to strongly depend on particle size [55]. Due to the relatively small nucleation rate of zirconolite crystals in the bulk of glass particles [55], no exothermic effect associated with bulk crystallization was observed during the DTA runs for GZr(Nd) and GHf(Nd)$_a$ glasses.

Study of glass-ceramics

Glass-ceramics with HfO_2

Crystallization in the bulk

The nature, microstructure and structure of crystalline phases formed in the bulk and near the surface (crystallized layer) of GHf and GHf(Nd)$_a$ glass-ceramic samples have been studied and compared to that of GZr and GZr(Nd) glass-ceramic samples containing only zirconium. SEM images of GHf(Nd)$_a$ glass-ceramic (bulk + surface) are shown in Fig. 4. The XRD pattern of the bulk of GHf glass-ceramic (T_c = 1,200 °C) is shown in Fig. 5.

The results of XRD and SEM studies are summarized in Table 4. The comparison of these results with that obtained for GZr and GZr(Nd) samples [25, 27] showed that the nature and the microstructure of the phases formed in the bulk or near the surface of were similar for glasses containing only ZrO_2 or HfO_2 (Figs. 4, 5). For all compositions, zirconolite remained the only crystalline phase nucleating in the bulk of the glass. The XRD pattern of the crystals formed in the bulk of GHf glass (T_c = 1,200 °C) was similar to that of a $CaHfTi_2O_7$ ceramic prepared by solid-state reaction at 1,460 °C [4, 37, 38] (Fig. 5). Moreover, the evolution with T_c of the microstructure of Hf-zirconolite crystals formed in the bulk—from dendritic (Fig. 4b) to elongated (Fig. 4e) morphology—was similar to that already observed and discussed for Zr-zirconolite crystals in GZr and GZr(Nd) glass-ceramics (compare Figs. 4a, e to c, f) [27,45].

The lattice parameters of Hf-zirconolite crystals formed at T_c = 1,050 °C in the bulk of GHf and GHf(Nd)$_a$ samples are given in Table 5. The corresponding XRD patterns were indexed in the monoclinic $C_{2/c}$ space group of the zirconolite-2M structure. Study of Table 5 showed that Hf-zirconolite crystals exhibited smaller (a,b,c) lattice parameters and cell volume V than Zr-zirconolite ones in GZr and GZr(Nd) samples. This result was in accordance with the (a,b,c,V) parameters increase observed for zirconolite ceramics when Hf was totally replaced by Zr (Table 5) [4, 37, 38]. This evolution could be explained by the fact that Hf^{4+} ion radius is slightly smaller than that of Zr^{4+} ion (Table 3). The introduction of neodymium in GHf glass composition induced an increase of (a,b,c,V)

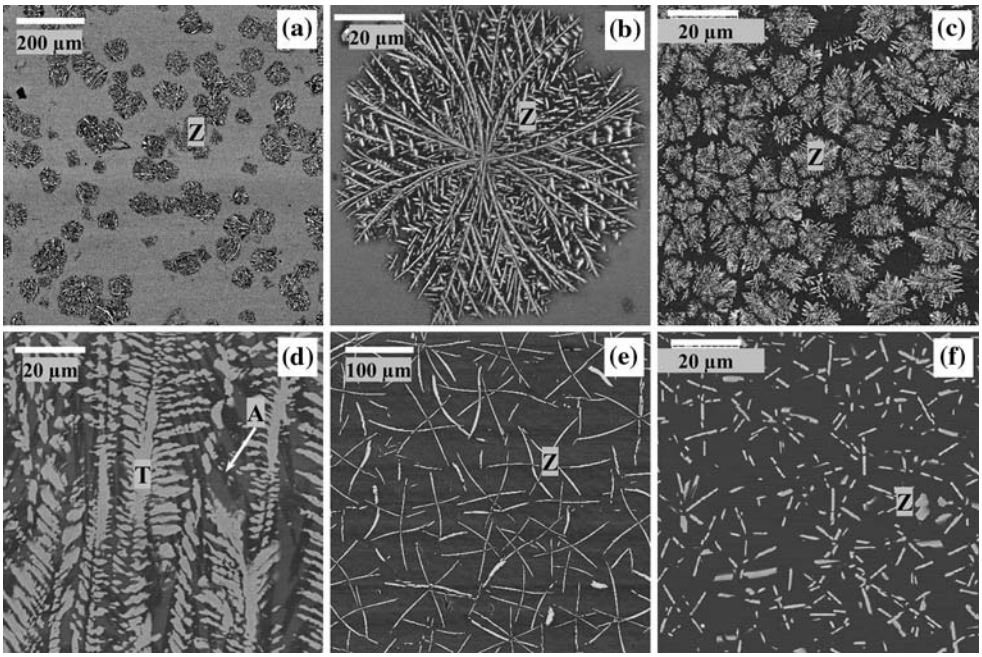

Fig. 4 Back-scattered SEM micrographs of bulk and surface of GHf(Nd)$_a$ glass-ceramic (T_n = 810 °C, 2 h): (**a**) and (**b**) bulk at T_c = 1,050 °C (2 h); (**d**) surface crystallized layer at T_c = 1,050 °C (2 h); (**e**) bulk at T_c = 1,200 °C (2 h). For comparison, the SEM micrographs of GZr(Nd) glass-ceramic (T_n = 810 °C, 2 h) are also presented: (**c**) bulk T_c = 1,050 °C (2 h); (**f**) bulk T_c = 1,200 °C (2 h). Z: zirconolite, T: titanite, A: anorthite. It is important to notice the scales difference between the micrographs of GHf(Nd)$_a$ and GZr(Nd) samples. Due to high concentration of heavy elements (Zr, Hf, Nd) in zirconolite crystals, the contrast between crystals (white) and residual glass (black) is strong

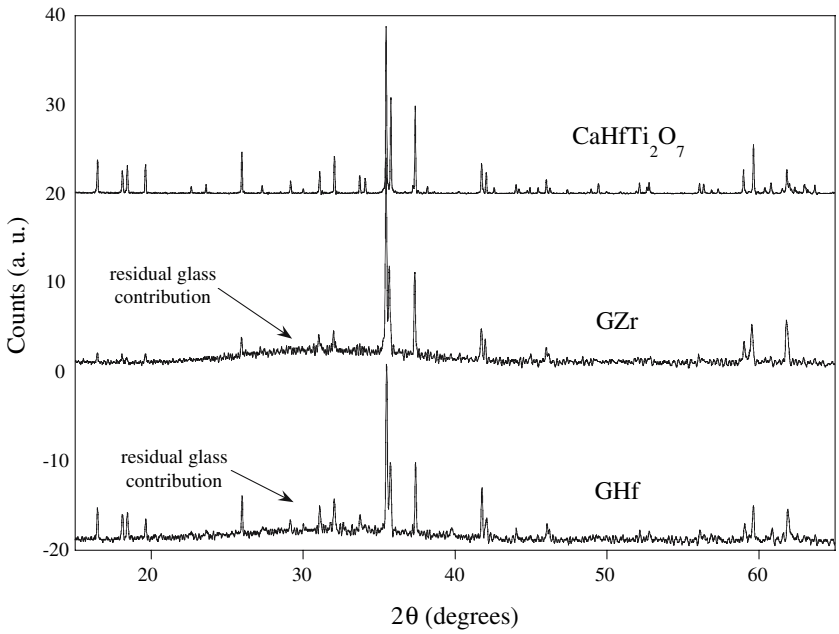

Fig. 5 XRD patterns (λ CoK_α) of the bulk of GZr and GHf glass-ceramics (T_n = 810 °C (2 h), T_c = 1,200 °C (2 h)). The XRD pattern of a $CaHfTi_2O_7$ ceramic synthesized at 1,460 °C is also given for comparison and shows that all the XRD lines observed on the glass-ceramic patterns are due to zirconolite crystals. The wide contribution to XRD pattern of residual glass in GZr and GHf glass-ceramics is shown

Table 4 Crystalline phases formed in the bulk and near the surface of GHf and $GHf(Nd)_a$ glass ceramics (T_n = 810 °C, 2 h). The crystal growth temperature (T_c) and duration are given in the first column of the Table

		Crystalline phases	Observations
1,050 °C (2 h)	Surface	T + A	Crystallized layer 1 mm thickness
1,050 °C (2 h)	Bulk	Z	Low nucleation rate, Z crystals 90 μm diameter
1,200 °C (2 h)	Surface	T + A	Crystallized layer 3 mm thickness
1,200 °C (2 h)	Bulk	Z	Low nucleation rate, Z crystals 150 μm diameter

T: titanite, A: anorthite, Z: zirconolite

parameters of Hf-zirconolite crystals (compare the results of GHf and $GHf(Nd)_a$ glass-ceramics in Table 5) which is in accordance with the results obtained for Nd-doped Zr-zirconolite based glass-ceramics studied previously [28, 37] (compare the lattice parameters of zirconolite crystals in GZr and GZr(Nd) glass-ceramics in Table 5). The composition of the Hf-zirconolite crystals formed at T_c = 1,200 °C in $GHf(Nd)_a$ glass was determined by EPMA (Table 6). From this composition the following formula was deduced: $Ca_{0.85}Nd_{0.21}Hf_{1.08}Ti_{1.71}Al_{0.18}O_7$ (Table 7). It is interesting to compare this formula with that of the Zr-zirconolite crystals formed in the bulk of the GZr(Nd) glass ceramic prepared following the same heat treatment: $Ca_{0.82}Nd_{0.19}Zr_{1.05}Ti_{1.77}Al_{0.17}O_7$ (determined by EDX analysis, Table 7) [56]. It appeared that Zr- and Hf-zirconolite crystals compositions were very similar because approximately 20% of the calcium sites of the structure were occupied by Nd^{3+} ions with charge compensation mainly insured by Al^{3+} ions in titanium sites. Consequently, the total replacement of Zr by Hf in parent glasses has no significant effect on the composition and on the structure of the zirconolite crystals formed in the bulk of glass-ceramics. Table 6 shows that the residual glass of $GHf(Nd)_a$ glass-ceramic is HfO_2 and TiO_2 depleted in comparison with parent glass because of zirconolite crystallization. Indeed, the atomic molar ratios Hf/Si and Ti/Si calculated from Table 6 decreased from 0.100 and 0.232 in $GHf(Nd)_a$ parent glass to respectively 0.056 and 0.156 in residual glass at T_c = 1,200 °C. Similarly, the atomic molar ratios Zr/Si and Ti/Si decreased from 0.101 and 0.231 in GZr(Nd) parent glass to respectively 0.044 and 0.137 in residual glass at T_c = 1,200 °C [27]. These results show that the amount of hafnium in the residual glass of $GHf(Nd)_a$ glass-ceramic is slightly higher than the amount of zirconium in the residual glass of GZr(Nd) glass-ceramic. This difference could indicate that HfO_2 was slightly more soluble than ZrO_2 in the glass/undercooled melt studied in this work. Concerning neodymium, the Nd/Si ratio in $GHf(Nd)_a$ and GZr(Nd) parent glasses decreased from 0.054 and 0.053 to respectively 0.045 and 0.045 in residual glass at T_c = 1,200 °C. This result showed that after crystallization, the residual glass was neodymium depleted because of the incorporation of a significant amount of Nd^{3+} ions in the crystalline phase. Unfortunately, for the application envisaged in this work, an important amount of neodymium (trivalent actinide surrogate) remained in the residual glass and would not benefit from a double containment barrier.

Figure 4 clearly shows that the nucleation rate of Hf-zirconolite crystals in $GHf(Nd)_a$ glass (Fig. 4a, e) is low

Table 5 Lattice parameters (a,b,c,β) and cell volume obtained by XRD of (Hf,Zr)-zirconolite crystals formed in the bulk of glass-ceramics containing HfO_2, ZrO_2 or HfO_2 + ZrO_2

Samples	a (Å)	b (Å)	c (Å)	β (°)	Volume (Å^3)
GHf	12.493 (3)	7.213 (1)	11.288 (2)	100.63 (1)	999.8 (3.3)
48 h 770 °C + 4 h 1,050 °C					
GZr	12.513 (2)	7.231 (1)	11.335 (1)	100.63 (1)	1008.1 (2.1)
2 h 810 °C + 2 h 1,050 °C					
$GHf(Nd)_a$	12.551 (2)	7.250 (1)	11.337 (3)	100.63 (3)	1013.9 (6.4)
2 h 810 °C + 2 h 1,050 °C					
GZr(Nd)	12.567 (3)	7.254 (2)	11.360 (3)	100.65 (3)	1017.8 (5.6)
2 h 810 °C + 2 h 1,050 °C					
GZr(Nd)	12.512 (2)	7.267 (1)	11.374 (2)	100.63 (2)	1016.4 (3.8)
2 h 810 °C + 2 h 1,200 °C					
$GZrHf(Nd)_a$	12.508 (3)	7.267 (2)	11.380 (2)	100.65(2)	1016.5 (3.9)
2 h 810 °C + 2 h 1,200 °C					
$Ca_{0.8}Nd_{0.2}HfTi_{1.8}Al_{0.2}O_7$ Ceramic	12.450	7.264	11.345	100.65 (4)	1008.3 (9)
$Ca_{0.8}Nd_{0.2}ZrTi_{1.8}Al_{0.2}O_7$ Ceramic	12.468	7.269	11.359	100.65 (5)	1011.9 (11)

The lattice parameters of $Ca_{0.8}Nd_{0.2}HfTi_{1.8}Al_{0.2}O_7$ and $Ca_{0.8}Nd_{0.2}ZrTi_{1.8}Al_{0.2}O_7$ ceramics prepared by solid-state reaction (100 h 1,400 °C + 100 h 1,460 °C) are also given for comparison [4, 37, 38]. The heat treatment conditions of glasses are indicated in the first column. Numbers in parentheses are standard deviations and apply to the last quoted place

in comparison with that of Zr-zirconolite crystals in GZr(Nd) glass (Fig. 4c, f). In order to compare more precisely Hf- and Zr-zirconolite nucleation rates, the nucleation rate curve $I_z = f(T)$ was determined for GHf glass and compared to that of GZr(Nd) glass determined in a previous study [26]. The corresponding curves are given in Fig. 6. It clearly appeared that the maximum of the nucleation rate curve was displaced towards lower temperature for GHf glass and decreased by approximately three orders of magnitude in comparison with GZr(Nd)

Table 6 Compositions (wt.%) determined by EPMA of the crystalline phases formed in the bulk (zirconolite) and near the surface (titanite, anorthite) of $GHf(Nd)_a$, $GZrHf(Nd)_a$, and $GZrHf(Nd)_b$ glasses heat treated at T_n = 810 °C (2 h) and T_c = 1,200 °C (2 h)

Samples	SiO_2	Al_2O_3	CaO	TiO_2	ZrO_2	HfO_2	Nd_2O_3	Na_2O
$GHf(Nd)_a$ (wt.%)								
Parent glass	38.17	10.97	18.84	11.82	0.09	13.49	5.78	0.83
Residual glass (bulk)	43.48	12.36	19.82	9.07	0.05	8.72	5.54	0.95
Zirconolite (bulk)	0.00	1.97	10.40	29.85	0.28	49.76	7.66	0.05
Titanite (surface)	24.32	3.17	20.77	21.13	0.06	22.99	7.47	0.07
Anorthite (surface)	49.80	30.54	15.99	0.65	0.00	0.37	0.28	2.35
$GZrHf(Nd)_a$ (wt.%)								
Parent glass	39.64	12.12	19.17	11.54	4.08	6.63	5.84	0.93
Residual glass (bulk)	44.52	12.79	20.35	9.08	2.28	4.22	5.76	0.98
Zirconolite (bulk)	0.00	2.00	11.87	33.79	18.16	25.78	8.37	0.00
Titanite (surface)	26.57	3.32	21.71	22.14	6.30	11.63	8.20	0.11
Anorthite (surface)	50.11	31.26	15.79	0.47	0.00	0.00	0.01	2.34
$GZrHf(Nd)_b$ (wt.%)								
Parent glass	37.69	10.80	18.42	11.57	8.22	6.64	5.88	0.76
Residual glass (bulk)	46.33	13.05	20.87	7.61	2.80	2.90	5.49	0.94
Zirconolite (bulk)	3.28	3.10	13.02	32.28	22.35	18.18	7.19	0.00
Titanite (surface)	25.11	2.54	21.92	23.06	9.84	10.01	7.52	0.00
Anorthite (surface)	48.62	31.12	15.36	0.54	1.56	0.66	0.00	2.12

The composition of parent glass and residual glass remaining between zirconolite crystals in the bulk of the glass-ceramics is also given for the three samples

Table 7 Composition deduced from EPMA and EDX results of zirconolite and titanite + anorthite crystals formed respectively in the bulk and near the surface of $GHf(Nd)_a$, $GZrHf(Nd)_a$, $GZrHf(Nd)_b$, and GZr(Nd) samples

Sample and crystalline phase	Formula
$GHf(Nd)_a$ zirconolite	$Ca_{0.85}Nd_{0.21}Hf_{1.08}Ti_{1.71}Al_{0.18}O_7$
GZr(Nd) zirconolite	$Ca_{0.82}Nd_{0.19}Zr_{1.05}Ti_{1.77}Al_{0.17}O_7$
$GZrHf(Nd)_a$ zirconolite	$Ca_{0.86}Nd_{0.20}Zr_{0.60}Hf_{0.49}Ti_{1.71}Al_{0.16}O_7$
$GZrHf(Nd)_b$ zirconolite	$Ca_{0.85}Nd_{0.18}Zr_{0.77}Hf_{0.37}Ti_{1.66}Al_{0.17}O_7$
$GHf(Nd)_a$ titanite	$Ca_{0.88}Nd_{0.11}Ti_{0.63}Hf_{0.26}Al_{0.15}Si_{0.97}O_5$
GZr(Nd) titanite	$Ca_{0.89}Nd_{0.11}Ti_{0.69}Zr_{0.22}Al_{0.11}Si_{0.98}O_5$
$GZrHf(Nd)_a$ titanite	$Ca_{0.90}Nd_{0.11}Ti_{0.67}Zr_{0.12}Hf_{0.14}Al_{0.11}Si_{0.95}O_5$
$GZrHf(Nd)_b$ titanite	$Ca_{0.90}Nd_{0.10}Ti_{0.66}Zr_{0.19}Hf_{0.11}Al_{0.10}Si_{0.94}O_5$
$GHf(Nd)_a$ anorthite	$Ca_{0.79}Na_{0.21}Al_{1.70}Si_{2.27}O_8$
GZr(Nd) anorthite	$Ca_{0.75}Na_{0.25}Al_{1.75}Si_{2.25}O_8$
$GZrHf(Nd)_a$ anorthite	$Ca_{0.77}Na_{0.21}Al_{1.69}Si_{2.29}O_8$
$GZrHf(Nd)_b$ anorthite	$Ca_{0.77}Na_{0.19}Al_{1.73}Si_{2.30}O_8$

All the samples were heat-treated at T_n = 810 °C (2 h) and T_c = 1,200 °C (2 h)

glass. This strong difference between the two samples was not due to the occurrence of neodymium in GZr(Nd) glass because we already showed that the nucleation rate of Zr-zirconolite decreased by increasing Nd_2O_3 amount [56]. The following reasons can be given to explain the zirconolite nucleation rate difference between glasses containing hafnium and zirconium:

– First, this difference could be due to the higher solubility of HfO_2 in comparison with ZrO_2 in the undercooled melt. Indeed, results reported in literature [57] concerning the solubility at 1,400 °C of ZrO_2 and HfO_2 in high silica liquids of the system SiO_2–Al_2O_3–Na_2O–K_2O showed that hafnium oxide was slightly more soluble than zirconium oxide. The same tendency could occur in our glass system. This solubility difference between ZrO_2 and HfO_2 seems to be confirmed by the study of crystallization near samples surface at T_c = 1,200 °C (see bellow). Indeed, whereas ZrO_2 crystallization was observed in GZr and GZr(Nd) glasses, HfO_2 crystals were not detected in glasses containing hafnium. This difference of solubility would thus indicate that Hf^{4+} ions activity was lower than Zr^{4+} ions activity in the undercooled melt thus leading to a lower zirconolite crystallization driving force and to a higher thermodynamic barrier for nucleation in the composition containing hafnium.
– Second, the strong mass difference between Hf^{4+} (M = 178.5 g mol^{-1}) and Zr^{4+} (M = 91.2 g mol^{-1}) ions probably induced more difficulties during nucleation for Hf^{4+} ions to diffuse in the undercooled melt than for Zr^{4+} ions. Indeed, it is known that for two isotopes A and B of a given element (with m_A and m_B the mass isotopes), the ratio of the diffusion coefficients D_A and D_B is such that [58]:

$$D_B/D_A = f(m_A/m_B)^{1/2} \quad (1)$$

Thus, if we consider hafnium and zirconium as two "pseudo-isotopes" (due to the similitude of their cation charge, their radius and their environment in glasses, Table 3), it leads to $D_{Hf}^{4+} < D_{Zr}^{4+}$. Consequently, the kinetic barrier for Hf-zirconolite nucleation is expected to be higher than for Zr-zirconolite nucleation.

Consequently, both thermodynamic (solubility difference between hafnium and zirconium in the undercooled melt) and kinetic (more difficulty for Hf^{4+} ions than for Zr^{4+} ions to diffuse in the undercooled melt) considerations can be given to explain the decrease of zirconolite nucleation rate when zirconium is totally replaced by hafnium in parent glass composition.

From SEM micrographs (Fig. 4a, b), it was possible to estimate the crystal growth rate of Hf-zirconolite crystals in the bulk using the diameter of the spherulitic shape non-impinging crystals formed at T_c = 1,050 °C. Assuming a linear dependency with time of the zirconolite crystal growth rate u_Z at T_c = 1,050 °C (as it is generally observed for spherulitic or dendritic crystal growth [59]), we found $u_Z \sim 0.4$ μm min^{-1} in $GHf(Nd)_a$ glass. The same u_Z value was obtained for GZr(Nd) glass which shows that contrary to nucleation rate, total replacement of Zr by Hf in parent glass composition has no effect on the zirconolite crystal growth rate.

In order to study the effect of T_c on the structure of crystals formed in the bulk of $GHf(Nd)_a$ sample and to make comparison with the crystals formed in GZr(Nd) sample containing only ZrO_2, other heat treatments were performed at T_c = 900 °C (8 h) and 950 °C (4 h) after

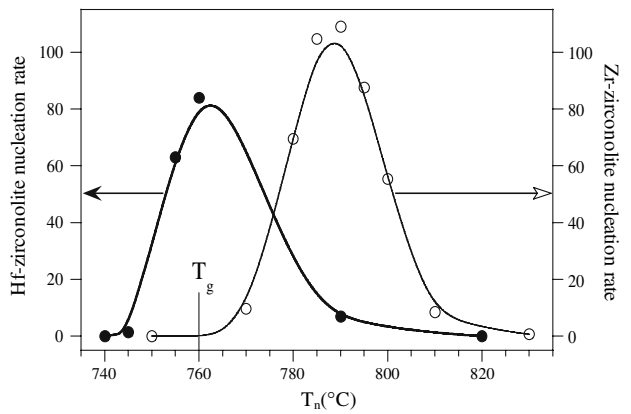

Fig. 6 Hf- and Zr-zirconolite crystals nucleation rate curves $I_z = f(T)$ respectively in GHf (number of nuclei cm^{-3} s^{-1}) and GZr(Nd) (number of nuclei mm^{-3} s^{-1}) glasses. It is important to notice the difference of ordinate scale between the two samples

nucleation at T_n = 770 °C (48 h). XRD showed that, similarly to the results obtained for GZr(Nd) glass [26, 27]:

- At T_c = 900 °C, a defect-fluorite phase crystallized in the bulk. This phase is a highly cation disordered zirconolite as described in [54].
- At T_c = 950 °C, a mixture of Hf-zirconolite and fluorite crystals was observed but the fluorite phase was no more detected at T_c = 1,050 °C. This structural evolution was due to the increase of cation ordering in fluorite-type phase when T_c increases in the 900–1,050 °C temperature range leading to the fluorite → zirconolite irreversible transformation.

Attempts to increase the amount of Hf-zirconolite crystals in the bulk of glass-ceramics

The comparison of the nucleation temperature chosen above (T_n = 810 °C) to prepare Hf-zirconolite based glass-ceramics with that of the maximum of the $I_z = f(T)$ curve of GHf glass reveals that T_n was not optimal for nucleation (Fig. 6). The annealing thermal treatment at 775 °C was probably more efficient than the heat treatment at 810 °C to induce the formation of Hf-zirconolite nuclei. Thus, in order to increase the amount of nuclei in $GHf(Nd)_a$ sample, the parent glass was nucleated at T_n = 770 °C for 48 h followed by a crystal growth heat treatment at T_c = 1,050 °C for 4 h. The SEM image of the bulk of the corresponding glass-ceramic is shown in Fig. 8a. By comparison with Fig. 4a, it appears that this new thermal treatment only leads to a slight increase of the number of crystals. However, because of the longer crystal growth duration (4 h), the amount of Hf-zirconolite phase was higher because of the increase of crystals size.

As the increase of the duration of nucleation had only small effect on the number of Hf-zirconolite nuclei in $GHf(Nd)_a$ glass, composition changes were performed by increasing either Al_2O_3 or HfO_2 concentrations in order to raise I_z. Indeed, we showed in previous works that the variation of Al_2O_3 concentration in GZr(Nd) glass had a strong effect on Zr-zirconolite nucleation rate in the bulk [29, 60]. Indeed, for GZr(Nd) glass composition, the increase of Al_2O_3 concentration by approximately 3 mol.% induced a strong increase of I_z [60]. Similarly, in the present study we prepared $GHf(Nd)_c$ glass by increasing Al_2O_3 concentration of nearly 3 mol.% in comparison with $GHf(Nd)_a$ (Table 1). The SEM image of the bulk of the glass-ceramics prepared at T_c = 1,050 °C is shown in Fig. 8b. An increase of I_z was observed in agreement with the results obtained for the glass containing only ZrO_2 but the effect observed here was lower than for this glass. The increase of I_z with Al_2O_3 concentration can be attributed to the decrease of HfO_2 and TiO_2 solubility in the undercooled melt which can be explained by the existence of a competition between Al^{3+} and (Hf^{4+},Ti^{4+}) ions—in favor of aluminum—for association with Na^+ and Ca^{2+} ions charge compensators [60]. Consequently, for the application envisaged in this study, Al_2O_3 concentration in parent glass could be raised in order to increase the Hf-zirconolite nucleation rate at least at T_c = 1,050 °C. However, the EDX results reported in [60] revealed that a high quantity of neodymium remained in residual glass.

In order to try to increase I_z, the amount of HfO_2 in parent glass $GHf(Nd)_a$ was also raised by 50% whereas the relative concentrations of other oxides were kept constant ($GHf(Nd)_b$ composition, Table 1). This composition change was performed to raise HfO_2 oversaturation in the undercooled melt and thus to increase Hf-zirconolite nucleation and crystal growth rates. The SEM micrographs of the bulk of the glass-ceramics prepared at T_c = 1,050 and 1,200 °C (2 h) are given in Fig. 8c, d. Comparison of Figs. 4a, e and 8c, d revealed that I_z was only slightly raised when HfO_2 concentration increased in parent glass. Whereas Hf-zirconolite remains the only phase to nucleate and to grow in the bulk at T_c = 1,050 °C, HfO_2 crystals are detected at T_c = 1,200 °C in the bulk (Fig. 8d).

Thus, the different composition changes (increase of Al_2O_3 or HfO_2 concentrations) performed in this study to increase the nucleation rate of Hf-zirconolite only lead to small I_Z evolution. This is the reason why, we decided to introduce simultaneously ZrO_2 and HfO_2 in glass composition because of the higher nucleating power of zirconium oxide (see below).

Partitioning of neodymium between Hf-zirconolite and residual glass in the bulk

Using ESR, the partitioning ratio R of neodymium ions between zirconolite crystals and residual glass in the bulk of $GHf(Nd)_a$ glass-ceramic prepared at T_c = 1,200 °C was estimated (Fig. 7, Table 8): R ∼ 21%. At T_c = 1,050 °C, the amount of crystals was too low to allow to estimate R. For comparison, R ∼ 24% for GZr(Nd) glass-ceramic prepared at T_c = 1,200 °C [37]. Thus, in spite of strong differences between Hf- and Zr-zirconolite nucleation rates, glasses containing Hf or Zr lead to approximately the same amount of neodymium ions incorporated in the crystalline phase in the bulk. This result indicated that for these two glass-ceramics, the amounts of zirconolite formed in the bulk at T_c = 1,200 °C were close because the number of Nd^{3+} ions incorporated in Hf- and Zr-zirconolite crystals by formula unit were very similar (respectively 0.21 and 0.19 in GZr(Nd) and $GHf(Nd)_a$ glass-ceramics) (Table 7). Moreover, the ESR spectrum of Hf-zirconolite

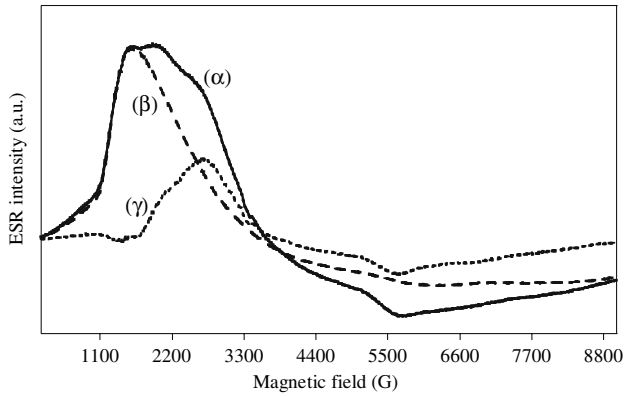

Fig. 7 ESR spectra recorded at T = 12 K (X-band) of the bulk of $GHf(Nd)_a$ glass-ceramic (α) prepared at T_c = 1,200 °C (2 h) showing the individual contributions of Nd^{3+} ions located in Hf-zirconolite crystals (γ) and in the residual glass (β) extracted following the method described in [28]

crystals formed in the bulk of $GHf(Nd)_a$ glass-ceramic prepared at 1200°C was very similar to that of a $Ca_{0.8}Nd_{0.2}HfTi_{1.8}Al_{0.2}O_7$ ceramic (prepared by solid state reaction at 1,460 °C, spectrum not shown) indicating that the local environment of Nd^{3+} ions in Hf-zirconolite crystals of the glass-ceramic was close to that of Nd^{3+} ions in the ceramic. This result was in accordance with EPMA and XRD results, which revealed that the composition and the structure of these crystalline phases were nearly identical. The partitioning ratio R in the bulk of $GHf(Nd)_b$ glass-ceramic (T_c = 1,200 °C, 2 h) was also determined: R ∼ 23%. This value was slightly higher than that determined for $GHf(Nd)_a$ sample but close to that of GZr(Nd) glass all heat treated at 1,200 °C (2 h) (Table 8).

Table 8 Partitioning ratio R estimated by ESR of neodymium ions between zirconolite crystals and residual glass in the bulk of the glass-ceramics

Sample	R
$GHf(Nd)_a$	21
2 h T_n = 810 °C + 2 h T_c = 1,200 °C	
$GHf(Nd)_b$	23
1 day T_n = 770 °C + 2 h T_c = 1,200 °C	
$GZrHf(Nd)_a$	32
2 h T_n = 810 °C + 2 h T_c = 1,050 °C	
1 day T_n = 760°C + 2 h T_c = 1,200 °C	24
$GZrHf(Nd)_b$	41
2 h T_n = 810 °C + 2 h T_c = 1,050 °C	
2 h T_n = 810 °C + 2 h T_c = 1,200 °C	30
GZr(Nd)	36
2 h T_n = 810 °C + 2 h T_c = 1,050 °C	
2 h T_n = 810 °C + 2 h T_c = 1,200 °C	24

The thermal treatment conditions used to prepare the glass-ceramics are given. The origin of the decrease of R with T_c was explained in [28]

Surface crystallization

XRD, SEM and EPMA results (Tables 4, 6, Fig. 4d) showed that titanite (nominally $CaTiSiO_5$) and anorthite (nominally $CaAl_2Si_2O_8$) were the only crystalline phases formed in the crystallized layer near the surface of GHf and $GHf(Nd)_a$ glass-ceramics at T_c = 1,050 or 1,200 °C. These two crystalline phases nucleated heterogeneously on samples surface and then grew towards the bulk. Their microstructure was similar to that of titanite and anorthite crystals grown in GZr and GZr(Nd) glasses [30]. However, contrary to GZr and GZr(Nd) glass-ceramics for which baddeleyite (ZrO_2) crystals were observed between titanite and anorthite crystals in residual glass near the surface (T_c = 1,200 °C) [30], HfO_2 crystals were not detected in GHf and $GHf(Nd)_a$ glass-ceramics. This difference could be explained by the higher solubility of HfO_2 in residual glass in comparison with ZrO_2 (see above). Due to the increase of titanite and anorthite crystal growth rates with temperature, the layer thickness e increased with T_c (Table 4). Moreover, e was higher for the glass-ceramics containing only HfO_2 (e = 1 and 3 mm at respectively T_c = 1,050 and 1,200 °C) than for the glass-ceramics containing only ZrO_2 (e = 150–200 and 800–900 μm at respectively T_c = 1,050 and 1,200 °C). This thickness difference could be explained by the small number of Hf-zirconolite crystals formed in the bulk of glass-ceramic containing only HfO_2. Hf-zirconolite crystals thus less disturbed the growth of titanite and anorthite crystals towards the bulk than the high number of Zr-zirconolite crystals in glass-ceramic containing only ZrO_2.

The following compositions were deduced from EPMA results (Tables 6, 7) respectively for titanite and anorthite in $GHf(Nd)_a$ glass-ceramic prepared at T_c = 1,200 °C (2 h): $Ca_{0.88}Nd_{0.11}Ti_{0.63}Hf_{0.26}Al_{0.15}Si_{0.97}O_5$ and $Ca_{0.79}Na_{0.21}Al_{1.70}Si_{2.27}O_8$. The corresponding compositions of titanite and anorthite crystals determined by EDX for GZr(Nd) glass-ceramic (T_c = 1,200 °C, 2h) were respectively: $Ca_{0.89}Nd_{0.11}Ti_{0.69}Zr_{0.22}Al_{0.11}Si_{0.98}O_5$ and $Ca_{0.75}Na_{0.25}Al_{1.75}Si_{2.25}O_8$ [26, 28]. The composition of silicate phases growing from glass surface were thus very similar for $GHf(Nd)_a$ and GZr(Nd) samples. Nd^{3+} ions are incorporated into the 7-fold coordinated calcium site of titanite crystals and charge compensation is insured by the simultaneous incorporation of Al^{3+} ions in the tetravalent sites of the structure. As for the glass containing only zirconium, crystals composition revealed that a significant amount of Hf^{4+} ions entered into the titanium six-fold

coordinated site of titanite. The fact that the amount of zirconium in titanite crystals of GZr(Nd) glass-ceramic was slightly lower that that of hafnium in titanite crystals of $GHfNd)_a$ glass-ceramic was probably due to the slightly smaller size of Hf^{4+} ions in comparison with Zr^{4+} ions (Table 3). Thus, the incorporation of Zr^{4+} ions into the six-fold coordinated Ti^{4+} site (0.605 Å [32]) of titanite would be slightly more difficult for than for Hf^{4+} ions. Table 7 reveals that anorthite crystals do not incorporate neither Nd^{3+} nor Hf^{4+} ions in their structure but can accept significant sodium concentration.

It is important to underline here that titanite (alternative name, sphene) is a phase known for its good incorporation capacity (Th, U, rare earth elements...) and good long-term behavior in spite of its tendency to become amorphous under self-radiation (existence of very old amorphous natural analogue) [23]. Titanite-based glass-ceramics were also proposed for nuclear waste immobilization in Canada [23, 24, 61]. Thus, the formation of this phase in our study—which incorporates high amounts of trivalent actinide surrogate near samples surface is not damaging for the waste form application envisaged in this work.

Glass-ceramics with both HfO_2 and ZrO_2

In order to study the effect of simultaneous introduction of both HfO_2 and ZrO_2 in parent glass on zirconolite crystals composition and nucleation rate, two parent glass compositions were prepared: $GZrHf(Nd)_a$ and $GZrHf(Nd)_b$ (Table 1).

In a first step, half of HfO_2 was replaced by ZrO_2 (in mol.%) in $GHf(Nd)_a$ composition ($GZrHf(Nd)_a$ sample). After heat treatment, zirconolite remained the only crystalline phase in the bulk as revealed by XRD (pattern not shown) but SEM did not revealed significant increase of the amount of zirconolite crystals in comparison with $GHf(Nd)_a$ sample after nucleation at T_n = 810 °C and crystal growth at T_c = 1,050 °C (micrographs not shown). This last result indicated that the introduction of 2.45 mol.% ZrO_2 in glass composition was not sufficient to increase I_Z. The zirconolite lattice parameters obtained for the glass-ceramic prepared at 1,200 °C (2 h) are given in Table 5. The comparison of these lattice parameters with those of the GZr(Nd) glass-ceramic (T_c = 1,200 °C, Table 5) indicates that they are very close. As for the glass-ceramics containing only ZrO_2 or HfO_2, titanite and anorthite formed a crystallized layer near sample surface. The composition of the different crystalline phases (bulk + surface) and of the residual glass in the bulk (T_c = 1,200 °C) were determined by EPMA and are given in Tables 6 and 7. The following formulas were obtained for the crystalline phases: $Ca_{0.86}Nd_{0.20}Zr_{0.60}Hf_{0.49}Ti_{1.71}Al_{0.16}O_7$ (zirconolite), $Ca_{0.90}Nd_{0.11}Ti_{0.67}Zr_{0.12}Hf_{0.14}Al_{0.11}Si_{0.95}O_5$ (titanite) and $Ca_{0.77}Na_{0.21}Al_{1.69}Si_{2.29}O_8$ (anorthite). The study of these compositions showed that:

- Both hafnium and zirconium entered into the structure of zirconolite crystals ((Hf,Zr)-zirconolite). However, the Zr/Hf molar ratios were respectively 1.22, 0.91, and 1.07 for zirconolite crystals, residual glass, and parent glass (all ratios deduced from EPMA results). Thus, the residual glass in the bulk was more depleted in Zr than in Hf. This result clearly showed that the partitioning ratios of zirconium and hafnium between the undercooled melt (i.e., the residual glass in the glass-ceramic samples) and the zirconolite crystals were different. This result was in agreement with the higher solubility of HfO_2 in comparison with ZrO_2 in the undercooled melt as suspected from our zirconolite nucleation rate study (see above) and from literature [57]. Moreover, the mass difference between Zr^{4+} and Hf^{4+} ions and thus the higher difficulty of Hf^{4+} ions to diffuse from the undercooled melt to the growing zirconolite crystals could also explain that Zr/Hf > 1 in the crystalline phase.
- The amount of Nd^{3+} ions incorporated into the zirconolite crystals of $GZrHf(Nd)_a$ sample remained very similar to that of the samples with only ZrO_2 (GZr(Nd)) or HfO_2 ($GHf(Nd)_a$). In this case, the charge compensation was also mainly insured by Al^{3+} ions. The partitioning ratio R of neodymium ions between zirconolite crystals and residual glass in the bulk of $GZrHf(Nd)_a$ glass-ceramic was estimated by ESR: R ≈ 32% (T_c = 1,050 °C, 2 h) and R ≈ 24% (T_c = 1,200 °C, 2 h) (Table 8).
- The amount of Zr^{4+} + Hf^{4+} ions incorporated into the zirconolite crystals of $GZrHf(Nd)_a$ sample was 1.09 (by formula unit). This quantity was very similar to the corresponding value of GZr(Nd) and $GHf(Nd)_a$ samples (respectively 1.05 and 1.08). Consequently, partial or total substitution of zirconium by hafnium in glass composition had no significant effect on the composition of zirconolite crystals.
- Concerning titanite crystals, it also appeared that partial or total substitution of zirconium by hafnium had no significant effect on their composition. Indeed, the amount of Nd^{3+} ions incorporated into titanite crystals (0.11 by formula unit) was the same for the three samples $GHf(Nd)_a$, $GZrHf(Nd)_a$, and GZr(Nd). However, contrary to zirconolite, the amount of Zr^{4+} and Hf^{4+} ions in titanite crystals (by formula unit) are so that Zr/Hf = 0.86 < 1. This preferential incorporation of hafnium could be due to the slightly higher capacity of titanium site in titanite structure to incorporate Hf^{4+}

ions as suspected above, comparing the composition of titanite crystals in $GHf(Nd)_a$ and GZr(Nd) glass-ceramics.
– Concerning anorthite crystals, their composition remained almost the same for the three samples $GHf(Nd)_a$, $GZrHf(Nd)_a$, and GZr(Nd).

In a second step, HfO_2 was added to GZr(Nd) glass composition with $[HfO_2]/[ZrO_2] = 0.5$ ($GZrHf(Nd)_b$ composition, Table 1). In this case, the amount of (Zr^{4+} + Hf^{4+}) ions was increased by a factor 1.5 in comparison with all previous compositions. SEM micrographs showed that the zirconolite nucleation rate in the bulk strongly increased for this composition following the order: $I_z(GHf(Nd)_a) < I_z(GZr(Nd)) < I_z(GZrHf(Nd)_b)$ (Fig. 8). At T_c = 1,050 °C, zirconolite still remained the only crystalline phase growing in the bulk of $GZrHf(Nd)_b$ glass-ceramic. However, at T_c = 1,200 °C two crystalline phases (zirconolite + $(Hf,Zr)O_2$) were observed in the bulk (Fig. 8f). The occurrence of this new crystalline phase (with baddeleyite structure) in $GZrHf(Nd)_b$ sample could be explained by the higher oversaturation of $(Hf,Zr)O_2$ in the undercooled melt due to the increase of ZrO_2 + HfO_2 concentration. It is interesting to underline that the crystallization of ZrO_2 was also observed in the bulk of GZr(Nd) glass-ceramics but only when T_c > 1,200 °C [30]. Consequently, the increase of ZrO_2 + HfO_2 concentration displaced baddeleyite crystallization towards lower temperature. As for all previous glass compositions, the crystallization of titanite and anorthite was also observed on $GZrHf(Nd)_b$ sample surface. At T_c = 1,200 °C, the composition of zirconolite (bulk), titanite, and anorthite crystals was determined by EPMA (Table 7): $Ca_{0.85}Nd_{0.18}Zr_{0.77}Hf_{0.37}Ti_{1.66}Al_{0.17}O_7$, $Ca_{0.90}Nd_{0.10}Ti_{0.66}Zr_{0.19}Hf_{0.11}Al_{0.10}Si_{0.94}O_5$ and $Ca_{0.77}Na_{0.19}Al_{1.73}Si_{2.30}O_8$. The composition of residual glass (bulk) is given in Table 6. Nearly the same amount of Nd^{3+} ions as in all previous compositions was incorporated into zirconolite and titanite crystals (by formula unit) of $GZrHf(Nd)_b$ sample (Table 7) and Al^{3+} ions acted as charge compensators. The Zr/Hf molar ratios were respectively 2.08, 1.72, and 1.68 in zirconolite, titanite, and bulk residual glass (all deduced from EPMA results). The relative Zr depletion in residual glass (Zr/Hf < 2) could be explained as above using both hafnium solubility and diffusion considerations. The same explanation as for $GZrHf(Nd)_a$ sample could be given to understand the fact that Zr/Hf < 1 in titanite crystals. The composition of anorthite crystals ($Ca_{0.77}Na_{0.19}Al_{1.73}Si_{2.30}O_8$) also remained the same as in previous glass-ceramics (Table 7). Using ESR, the following

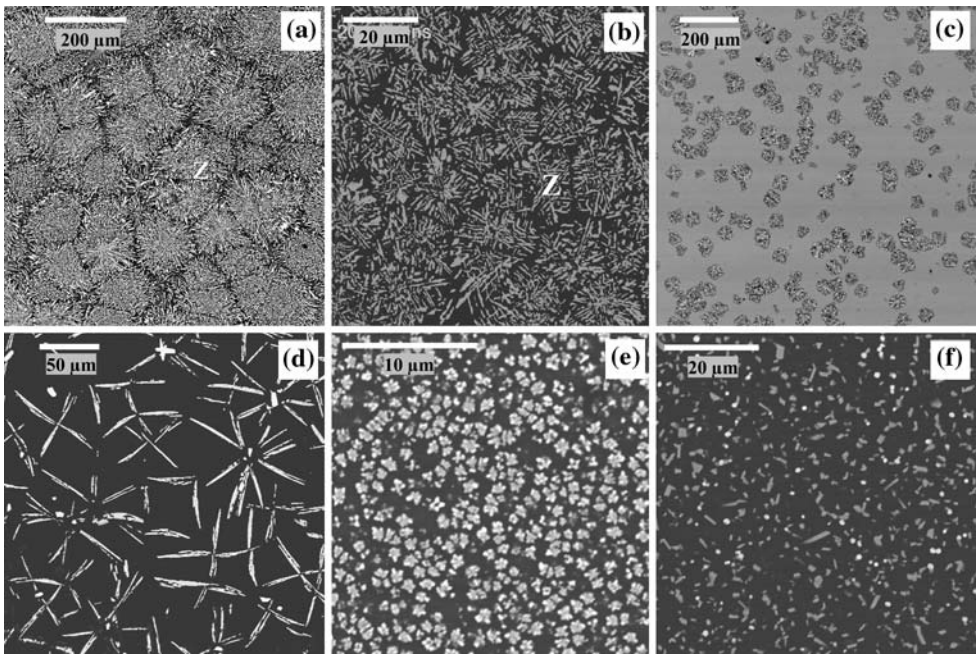

Fig. 8 Back-scattered SEM micrographs of the bulk of the glass-ceramic (Z: zirconolite): (**a**) $GHf(Nd)_a$ (T_n = 770 °C for 48 h and T_c = 1,050 °C for 4 h); (**b**) $GHf(Nd)_c$ (T_n = 810 °C for 2 h and T_c = 1,050 °C and 2 h); (**c**) $GHf(Nd)_b$ (T_n = 810 °C for 2 h and T_c = 1,050 °C for 2 h); (**d**) $GHf(Nd)_b$ (T_n = 810 °C for 2 h and T_c = 1,200 °C for 2 h); (**e**) $GZrHf(Nd)_b$ (T_n = 810 °C for 2 h and T_c = 1,050 °C for 2 h); (**f**) $GZrHf(Nd)_b$ (T_n = 810 °C for 2 h and T_c = 1,200 °C for 2 h). Zirconolite was the only crystalline phase formed in the bulk except in (**d**) and (**f**) where a mixture of zirconolite (gray crystals in (**f**) and elongated white crystals in (**d**)) and HfO_2/$(Zr,Hf)O_2$ (small isolated white crystals in (**d**) and white crystals in (**f**)) was observed. It is important to notice the scale difference between micrographs

partitioning ratio R in the bulk of $GZrHf(Nd)_b$ glass-ceramic was estimated: R ~ 41% (T_c = 1,050 °C, 2 h) and R ~ 30% (T_c = 1,200 °C, 2 h) (Table 8). These values were higher than those estimated for $GZrHf(Nd)_a$ and GZr(Nd) samples which could be explained by the higher amount of Zr^{4+} and Hf^{4+} ions available to form (Hf,Zr)-zirconolite nuclei in $GZrHf(Nd)_b$ sample.

Conclusions

Minor actinides are responsible for the main contribution to long-term radiotoxicity of high-level nuclear waste solutions obtained after nuclear spent fuel reprocessing. Zirconolite is a crystalline phase well known for its high performances for actinides immobilization. In previous works, we showed that it was possible to prepare glass-ceramics with Zr-zirconolite crystals as the only crystalline phase in the bulk by controlled crystallization of parent glasses containing high amounts of ZrO_2 + TiO_2. In this study, we showed that such glass-ceramics could be also prepared substituting either totally or partially zirconium by hafnium in glass composition. For crystal growth temperature 1,050 °C $\leq T_c \leq$ 1,200 °C, Hf- or (Hf,Zr)-zirconolite remained the main crystalline phase to nucleate in the bulk. At $T_c \leq$ 950 °C, a fluorite-type phase crystallized in the bulk. This phase corresponds to a cationic disordered zirconolite. Independently on glass composition, Nd^{3+} ions were partially incorporated into zirconolite crystals with charge compensation mainly insured by Al^{3+} ions. However, an important amount of neodymium remained in residual glass. The replacement of Zr by Hf had no significant effect on the nature of the crystalline phases nucleating heterogeneously on glass surface: titanite and anorthite phases growing towards bulk were always observed. Among these two phases, titanite was the only one able to incorporate neodymium. Contrary to the glass-ceramic with only ZrO_2, HfO_2 crystals were not detected in the crystallized layer at T_c = 1,200 °C for the glass-ceramic with only HfO_2. Moreover, strong differences were observed between Zr- and Hf-zirconolite nucleation rates. Indeed, the zirconolite nucleation rate in the bulk of the glass-ceramic with only HfO_2 decreased by approximately three orders of magnitude in comparison with the glass-ceramic with only ZrO_2. All these differences could be due both to the slightly higher solubility of hafnium in comparison with zirconium in undercooled melt (leading to a lower zirconolite crystallization driving force) and to the strong mass difference between Hf^{4+} and Zr^{4+} ions that would induce diffusion difficulties during nucleation. Modifications of thermal treatment conditions (duration, nucleation temperature) and parent glass composition changes were performed in order to try to increase the zirconolite nucleation rate in Hf-rich samples. The most efficient effects were obtained either by increasing Al_2O_3 concentration or by adding ZrO_2 in glass composition. Nevertheless, even for these compositions the quantity of Nd^{3+} ions (trivalent actinides surrogate) that remained in residual glass after zirconolite crystallization (and that would thus not benefit from a double containment barrier) was still to high to consider zirconolite-based glass-ceramics as waste form more efficient than zirconolite to immobilize minor actinides or plutonium.

Acknowledgements The CEA (Commissariat à l'Energie Atomique) and the French Group Nomade are gratefully acknowledged for their financial supports to this study. The authors would also like to thank C. Fillet (CEA Marcoule, France) for fruitful discussions.

References

1. Donald IW, Metcalfe BL, Taylor RN (1997) J Mater Sci 32:5851, DOI: 10.1023/A:1018646507438
2. Lee WE, Ojovan MI, Stennet MC, Hyatt NC (2006) Adv Appl Ceram 105:3
3. Ojovan MI, Lee WE (2005) An introduction to nuclear waste immobilisation. Elsevier, Oxford, UK
4. Caurant D, Loiseau P, Aubin-Chevaldonnet V, Gourier D, Majérus O, Bardez I (in press) In: Keister JE (ed) Nuclear materials research developments. Nova Science Publishers, Hauppauge, NY, USA
5. Guillaumont R (2004) C R Chimie 7:1129
6. Strachan DM, Scheele RD, Buck EC, Icenhower JP, Kozelisky AE, Sell RL, Elovich RJ, Buchmiller WC (2005) J Nucl Mater 345:109
7. Anderson EV, Burakov BE (2004) Mater Res Soc Symp Proc 807:207
8. Madic C, Lecomte M, Baron P, Boullis B (2002) C R Physique 3:797
9. Guy C, Audubert F, Lartigue JE, Latrille C, Advocat T, Fillet C (2002) C R Physique 3:827
10. Fillet C, Advocat T, Bart F, Leturcq G, Rabiller H (2004) C R Chimie 7:1165
11. Yudintsev SV (2003) Geol Ore Deposit 45:151
12. Laverov NP, Yudinstev SV, Yudintseva TS, Stefanovsky SV, Ewing RC, Lian J, Utsunomiya S, Wang LM (2003) Geol Ore Deposit 45:423
13. Dacheux N, Clavier N, Robisson AC, Terra O, Audubert F, Lartigue JE, Guy C (2004) C R Chimie 7:1141
14. Ochkin AV, Stefanosky SV, Ptashkin AG, Mikhailenko NS, Kirjanova OI (2004) Mater Res Soc Symp Proc 824:267
15. Ringwood AE, Kesson SE, Ware NG, Hibberson WO, Major A (1979) Geochem J 13:141
16. Smith KL, Zhang Z, McGlinn P, Attard D, Li H, Lumpkin GR, Colella M, McLeod T, Aly Z, Loi E, Leung S, Hart KP, Ridgway M, Weber WJ, Thevuthasan S (2003) Mater Res Soc Symp Proc 757:289
17. McGlinn PJ, Advocat T, Leturcq G, McLeod TI, Aly Z, Yee P (2006) Mater Res Soc Symp Proc 932:575
18. Leturcq G, McGlinn PJ, Barbe C, Blackford MG, Finnie KS (2005) Appl Geochem 20:899
19. Roberts SK, Bourcier WL, Shaw HF (2000) Radiochim Acta 88:539

20. Jorion F, Deschanels X, Advocat T, Desmouliere F, Cachia JN, Peuget S, Roudil D, Leturcq G (2006) Nucl Sci Eng 153:262
21. Fielding PE, White TJ (1987) J Mater Res 2:387
22. Xu H, Wang Y (2000) J Nucl Mater 279:100
23. Hayward PJ (1988) In: Lutze W, Ewing RC (eds) Radioactive waste forms for the future. North Holland, Amsterdam, The Netherlands, p 427
24. Hayward PJ (1988) Glass Technol 29:122
25. Caurant D, Majérus O, Loiseau P, Bardez I, Baffier N, Dussossoy JL (2006) J Nucl Mater 354:143
26. Loiseau P, Caurant D, Majérus O, Baffier N, Mazerolles L, Fillet C (2002) Phys Chem Glasses 43C:195
27. Loiseau P, Caurant D, Majérus O, Baffier N, Fillet C (2003) J Mater Sci 38:843, DOI: 10.1023/A:1021873301498
28. Loiseau P, Caurant D, Baffier N, Fillet C (2001) Mater Res Soc Symp Proc 663:169
29. Loiseau P, Caurant D, Bardez I, Majérus O, Baffier N, Fillet C (2003) Mater Res Soc Symp Proc 757:281
30. Loiseau P, Caurant D, Baffier N, Mazerolles L, Fillet C (2004) J Nucl Mater 335:14
31. Advocat T, Marcillat T, Deschanels X, Leturcq G, Jorion F, Rabiller H, Loiseau P, Veiller L (2002) In: Rabbe C, Vernaz E (eds) CEA Atalante: Rapport Scientifique 2002, Direction de l'énergie nucléaire (CEA-R-6800 ISSN 0429–3460), p 144
32. Shannon RD (1976) Acta Cryst A32:751
33. McCauley RA, Hummel FA (1980) J Solid State Chem 33:99
34. Swenson D, Nieh TG, Fournelle JH (1996) Mater Res Soc Symp Proc 412:337
35. Vance ER, Jostsons A, Day R, Ball CJ, Begg BD, Angel PJ (1996) Mater Res Soc Symp Proc 412:41
36. Putnam RL, Navrotsky A, Woodfield BF, Shapiro JL, Stevens R, Boerio-Goates J (1999) Mater Res Soc Symp Proc 556:11
37. Loiseau P (2001) PhD Thesis, Université Paris VI, France
38. Caurant D, Bardez I, Loiseau P (in preparation)
39. Hart KP, Vance ER, Stewart MW, Weir J, Carter ML, Hambley M, Brownscombe A, Day RA, Leung S, Ball CJ, Ebbinghaus B, Gray L, Kan T (1998) Mater Res Soc Symp Proc 506:161
40. Giéré R, Malmström J, Reusser E, Lumpkin GR, Düggelin M, Mathys D, Guggenheim R, Günther D (2001) Mater Res Soc Symp Proc 663:267
41. Emsley J (1992) In: The elements. Clarendon Press (Oxford), p 82 and p 220
42. Feng X, Li H, Li L, Darab JG, Schweiger MJ, Vienna JD, Bunker BC, Allen PG, Bucher JJ, Craig IM, Edelstein NM, Shuh DK, Ewing RC, Wang LM, Vance ER (1999) Ceram Trans 93:409
43. Helean KB, Navrotsky A, Vance ER, Carter ML, Ebbinghaus B, Krikorian O, Lian J, Wang LM, Catalano JG (2002) J Nucl Mater 303:226
44. Lumpkin GR, Whittle KR, Rios S, Smith KL, Zaluzec NJ (2004) J Phys Condens Matter 16:8557
45. Loiseau P, Caurant D, Baffier N, Mazerolles L, Fillet C (2001) Mater Res Soc Symp Proc 663:179
46. Osborn EF, Muan A (1964) Phase diagrams for ceramists. The American Ceramic Society, Columbus, OH, USA, p 219
47. Barton J, Guillemet C (2005) In: Le Verre: science et technologie. EDP Sciences, Les Ullis, France, p 180
48. McMillan PW (1979) In: Glass-ceramics. Academic Press, London, UK, p 61
49. Strnad Z (1986) In: Glass-ceramic materials, glass science and technology, vol 8. Elsevier, Amsterdam, The Netherlands, p 72
50. Bihuniak PP, Condrate RA (1981) J Non-Cryst Solids 44:331
51. Galoisy L, Pélegrin E, Arrio MA, Ildefonse P, Calas G (1999) J Am Ceram Soc 82:2219
52. Caulder DL, Booth CH, Bucher JJ, Edelstein NM, Liu P, Lukens WW, Rao L, Shuh DK, Davis LL, Darab JG, Li H, Li L, Strachan DM (2000) In: 219th American Chemical Society National Meeting. Division of Nuclear Chemistry and Technology, Symposium on Nuclear Waste Remediation and Long Term Storage, San Francisco, USA, 26–30 March 2000 (poster session)
53. Strachan DM, Shuh DK, Ewing RC, Vance ER (2001) Distribution and solubility of radionuclides and neutrons absorbers in waste forms for disposition of plutonium ash and scraps, excess plutonium and miscellaneous spent nuclear fuels, Final Report (US DOE), Project Number 60387
54. Vance ER, Ball CJ, Blackford MG, Cassidy DJ, Smith KL (1990) J Nucl Mater 175:58
55. Loiseau P, Caurant D, Majérus O, Baffier N, Fillet C (2003) J Mater Sci 38:853, DOI: 10.1023/A:1021825418336
56. Loiseau P, Caurant D, Baffier N, Fillet C (2002) Phys Chem Glasses 43C:201
57. Ellison AJ, Hess PC (1986) Contrib Mineral Petrol 94:343
58. Varshneya AK (1994) In: Fundamentals of inorganic glasses. Academic Press Inc., NY, USA, p 323
59. Kirkpatrick RJ, Klein L, Uhlmann DR, Hays JH (1979) J Geophys Res 84:3671
60. Caurant D, Bardez I, Loiseau P, Gervais C, J Mater Sci (in press)
61. Hayward PJ, Vance ER, Cann CD, Mitchell SL (1984) In: Wicks G, Ross WA (eds), Advances in ceramics, vol 8. The American Ceramic Society, Columbus, OH, p 291